THE ASTROPHYSICAL JOURNAL, 368: L27–L30, 1991 February 20

RAYLEIGH-TAYLOR INSTABILITIES AND MIXING IN THE HELIUM STAR MODELS FOR TYPE Ib/Ic SUPERNOVAE

IZUMI HACHISU AND TAKUYA MATSUDA
Department of Aeronautical Engineering, Kyoto University, Kyoto 606, Japan
AND
KEN'ICHI NOMOTO AND TOSHIKAZU SHIGEYAMA
Department of Astronomy, Faculty of Sciences, University of Tokyo, Bunkyo-ku, Tokyo 113, Japan
Received 1990 July 11; accepted 1990 November 14

ABSTRACT

Motivated by the necessity of large-scale mixing in modeling the light curves of Type Ib/Ic supernovae (SN Ib/Ic), the Rayleigh-Taylor (R-T) instabilities in exploding helium stars of masses $M_\alpha = 3.3$, 4, and 6 $M_\odot$ are calculated for the first time with a two-dimensional hydrodynamical code. Mixing of the ejected material induced by the instabilities is found to be more extensive for smaller mass stars. For $M_\alpha \lesssim 4\ M_\odot$, ^{56}Ni is mixed to the outermost helium envelope. For $M_\alpha \gtrsim 6\ M_\odot$, on the contrary, the growth of the R-T instability is too weak to convey ^{56}Ni into the outer layers. The extensive mixing in smaller mass stars is consistent with the early light curve models for SN 1983N (Type Ib) and SN 1987M (Type Ic) whose declines are as fast as and even faster than Type Ia supernovae. On the other hand, no significant mixing for larger M_α may be consistent with the slow decline of SN Ib 1984L. Thus the observed variation of the SN Ib/Ic light curves can naturally be accounted for by the variation of mixing as a function of the helium star mass.

Subject headings: hydrodynamics — instabilities — stars: supernovae

1. INTRODUCTION

Type Ib/Ic supernovae (SN Ib/Ic) have been suggested to be the explosion of Wolf-Rayet stars (see, e.g., Harkness & Wheeler 1990 for a review and references). However, the early bolometric light curves of SN Ib 1983N (Type Ib), which declines as fast as SN Ia (Panagia 1987), and of SN 1987M (Type Ic), declining even faster than SN Ia (Filippenko, Porter, & Sargent 1990), have been difficult to reproduce with the Wolf-Rayet star models (Ensman & Woosley 1988; Nomoto, Shigeyama, & Hashimoto 1988; Nomoto et al. 1988). Recently Shigeyama et al. (1990) and Nomoto, Filippenko, & Shigeyama (1990) have shown that the fast declines of the SN Ib/Ic light curves are well reproduced if mixing of ^{56}Ni occurs in 3–4 $M_\odot$ helium stars. Mixing and clumpiness in SN 1985F (Type Ib) are also suggested from the observed emission-line structures (Fransson & Chevalier 1989; Filippenko & Sargent 1989). On the other hand, the visual light curve of SN Ib 1984L declines at a rate close to the ^{56}Co decay rate for over ~ 600 days (Schlegel & Kirshner 1989). These variations of the SN Ib/Ic light curves indicate the presence of the different degree of mixing among SN Ib/Ic (Nomoto & Shigeyama 1990).

Such a mixing of radioactive elements has been observed in SN 1987A (e.g., Kumagai et al. 1989 and references therein) and successfully accounted for by the Rayleigh-Taylor (R-T) instability in the explosion (Arnett, Fryxell, & Müller 1989; Hachisu et al. 1990; Den, Yoshida, & Yamada 1990; Yamada, Nakamura, & Oohara 1990; Fryxell, Arnett, & Müller 1991; Müller, Fryxell, & Arnett 1990). The R-T instability develops when the expanding core materials undergo large deceleration due to the interaction with the massive low-density envelope. The instability grows fast at a composition interface which has the steepest density gradient (Ebisuzaki, Shigeyama, & Nomoto 1989; Benz & Thielemann 1990; Goodman 1990).

In the exploding helium stars, the instability would grow at the He/C + O interface due to the core deceleration by the helium envelope. Shigeyama et al. (1990) have performed linear stability analysis and suggested that the R-T instability would occur only for relatively low-mass helium stars but not for fairly massive models. In the present *Letter*, we perform for the first time two-dimensional simulations of the R-T instabilities in the exploding helium stars and confirm the occurrence of the R-T instabilities as well as the mass dependence.

2. INITIAL MODELS

Three progenitor models are examined. These are the helium stars of masses $M_\alpha = 6\ M_\odot$, $4\ M_\odot$, and $3.3\ M_\odot$ whose light curves and nucleosynthesis have been studied by Shigeyama et al. (1990). The final kinetic energy of explosion is $E = 1 \times 10^{51}$ ergs for all models. The composition structures, i.e., the locations of the composition interfaces in the adopted models are given in Table 1, while the masses of the neutron star and ejected ^{56}Ni (i.e., the location of the Si/Ni interface) are assumed as follows.

2.1. *The 6 $M_\odot$ Helium Star*

The neutron star mass is assumed to be 1.6 $M_\odot$ (Shigeyama, Nomoto, & Hashimoto 1988; Shigeyama & Nomoto 1990). The model has ejecta mass of $M_{ej} = 4.4\ M_\odot$ thereby being called 4.4E1, where E1 denotes $E = 1 \times 10^{51}$ ergs. The mass of ^{56}Ni is assumed to be 0.075 $M_\odot$ as inferred from SN 1987A. The neutron star mass and ^{56}Ni mass are consistent with the SN 1987A model (Hashimoto, Nomoto, & Shigeyama 1989; Thielemann, Hashimoto, & Nomoto 1990).

2.2. *The 4 and 3.3 $M_\odot$ Helium Stars*

The neutron star masses are equal to the iron core masses of 1.28 $M_\odot$ for $M_\alpha = 4\ M_\odot$ (model 2.7E1) and 1.18 $M_\odot$ for $M_\alpha = 3.3\ M_\odot$ (model 2.1E1) (Nomoto & Hashimoto 1988). The masses of ^{56}Ni are 0.15 $M_\odot$ for 2.7E1 and 0.26 $M_\odot$ for

TABLE 1

INITIAL MODELS

Model Name	M_{NS} ($M_\odot$)	$M_{Si/Ni}$ ($M_\odot$)	$M_{O/Si}$ ($M_\odot$)	$M_{He/C+O}$ ($M_\odot$)	M_{He} ($M_\odot$)	M_{ej} ($M_\odot$)
4.4E1.....	1.6	1.675	1.75	3.8	6.0	4.4
2.7E1.....	1.28	1.43	1.57	2.1	4.0	2.7
2.1E1.....	1.18	1.44	1.54	1.8	3.3	2.1

2.1E1 as obtained from the nucleosynthesis calculations (Shigeyama et al. 1990).

3. RAYLEIGH-TAYLOR INSTABILITIES AND MIXING

Early shock propagation from $t = 0$ to t_0 is calculated with the one-dimensional Lagrangian code (Shigeyama et al 1990). Then physical quantities such as densities, velocities, and internal energies are mapped onto the two-dimensional grids of our axisymmetric hydrodynamic code. After the mapping, the velocity field interior to the shock front is perturbed, while the velocities outside the shock remain zero. Two types of perturbation are applied: (1) periodic sinusoidal perturbation, which is represented by $1 + \epsilon \cos(m\theta)$, and (2) random perturbation where the latitudinal angle is divided into n pieces and the velocity field is perturbed at each π/n latitudinal angle. The amplitude of the perturbation is $\epsilon = 0.05$ for both cases. We refer to the models with a periodic perturbation of $m = 20$ as M20 and with a random one of $n = 128$ as R128. The source of perturbation could be convective motion in the convective helium-burning shell around the He/C + O interface. No prominent instabilities grew if we did not introduce finite perturbations mainly because the duration of the deceleration is too short for the growth of such a small amplitude perturbation as machine noise.

In the present two-dimensional calculations, we use 1729 × 1729 mesh points on a cylindrical coordinate system (R, Z) with an equal mesh interval $\Delta R = \Delta Z$ (see Table 2). The computational region covers $\theta = 0 - \pi/2$, and an equatorial symmetry is assumed. To examine the extent of mixing, we follow the positions of 3075 (or 12,291) marker particles which are initially placed at the He/C + O, O/Si, and Si/Ni interfaces. We solve the Euler equations with a constant adiabatic index $\gamma = 4/3$, which is a good approximation for the present radiation dominant situation. Our numerical method is the same one as used in Hachisu et al. (1990).

3.1. *The 6 $M_\odot$ Helium Star* (4.4E1)

We start our two-dimensional calculation from $t = t_0 =$ 9.0 s with a mode of M20 (run 1 of Table 2) when the blast shock has already arrived at the bottom of the helium layer. Figure 1 shows the density contour (*left*) and the positions of marker particles at each composition interface (*right*) at $t = 80$ s. The He/C + O interface is certainly R-T unstable, but its nonlinear growth is small as seen in Figure 1. The velocity

TABLE 2

MAXIMUM/MINIMUM VELOCITIES OF COMPOSITION INTERFACES AFTER THE SHOCK BREAKOUT

Number of Run	Initial Model	$\Delta R = \Delta Z$ (10^8 cm)	Time (s)	^{56}Ni (km s^{-1})	O/Si (km s^{-1})	He/C + O (km s^{-1})
1.....	4.4E1	0.32	100.	...	3090/2560	4900/3500
2.....	4.4E1	1.0	150.	...	...	5130/3590
3.....	2.7E1	0.89	170.	4650/1740	5460/1990	5670/2190
4.....	2.1E1	0.88	180.	7370/2130	7380/2150	7380/2290

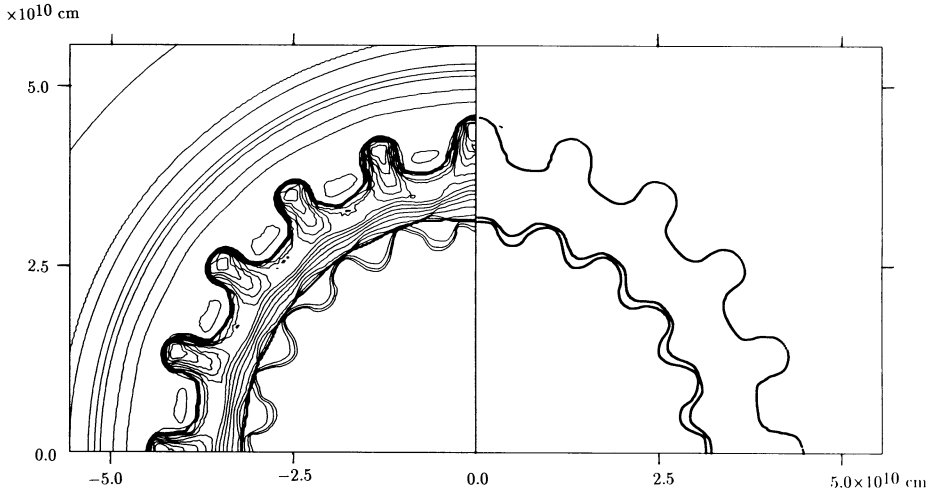

FIG. 1.—*Left*: Density contour map at $t = 80$ s after the explosion for run 1 (4.4E1). Each contour is linearly spaced by 5%. The vertical line through the center corresponds to the symmetry axis. The size of the plotted region is $5.5 \times 10^{10} \times 5.5 \times 10^{10}$ ($R \times Z$) cm^2. The forward shock has already moved out of the figure, while the reverse shock from the He/C + O interface has just reached the innermost contour. The density contour is mapped from the 1729 × 1729 mesh used in the calculations on to the 217 × 217 mesh, which degrade the quality of the contour. *Right*: Composition interfaces shown by marker particles. From the outside shown are the interfaces of He/C + O, O/Si, and Si/Ni. The first interface corresponds to the jump of the density contours in the left figure, but the O/Si and Si/Ni interfaces do not have a steep density gradient. The R-T instability is not so prominent at the He/C + O interface.

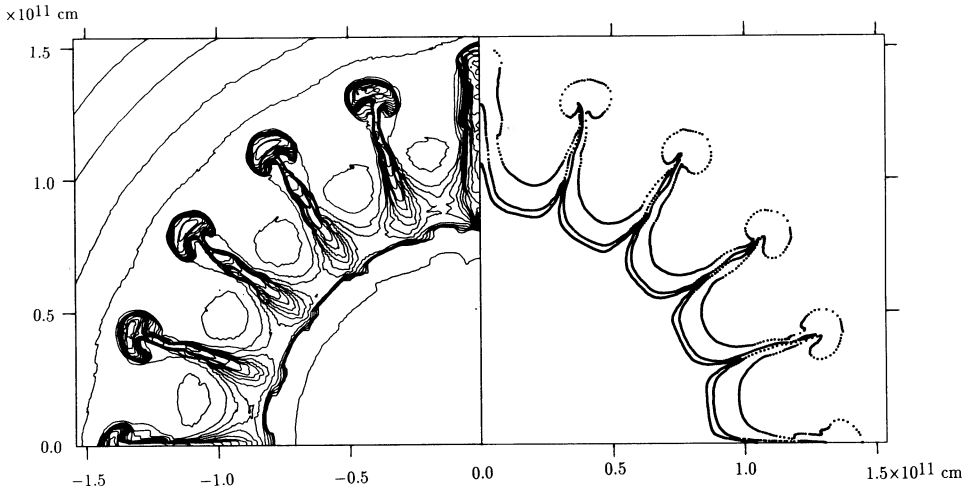

FIG. 2.—Same as Fig. 1 but for run 3 (2.7E1) at $t = 256$ s. *Left*: Density contour map. *Right*: Marker particles at the He/C + O, O/Si, and Si/Ni interfaces. The plotted region is $1.5 \times 10^{11} \times 1.5 \times 10^{11}$ cm^2. It is seen that the R-T instability is prominent and induces large scale mixing.

dispersion given in Table 2 increases from initial 10% to only 30%. Clearly the R-T mixing does not induce a large-scale mixing. This result does not depend much on the mesh size ΔR; in run 2 of Table 2 which assumes larger ΔR, the mushroom-like structures and the velocity dispersion at the He/C + O interface are not different from those for run 1.

3.2. *The* 4 $M_\odot$ *Helium Star* (2.7E1)

We start the calculation from $t = t_0 = 10$ s with a mode of M20 when the blast shock has already reached the bottom of the He envelope (run 3). Figure 2 shows the density contour and the positions of marker particles at $t = 256$ s. The shock has broken out of the stellar surface and no further growth of the R-T instability is expected. It is clearly seen that the R-T instability induces a large scale mixing in the ejecta. ^{56}Ni is mixed up to the layer of $M_r \sim 1.1\ M_\odot$, where M_r denotes the mass of the ejecta within the spherical radius r. The density contour shows that the density ratio between the mushroom heads and the surrounding media is 4–5, so that the mushroom features can be regarded as density clumps. Thus the R-T instabilities not only induce mixing but also form clumpy ejecta.

3.3. *The* 3.3 $M_\odot$ *Helium Star* (2.1E1)

As expected from the large density contrast between the carbon-oxygen core and the helium envelope, nonlinear development of the R-T instability is much more prominent than 2.7E1. Figure 3 shows the density contour and the marker particles for run 5 with a random perturbation (R128) and $t_0 = 10$ s, which is not tabulated in Table 2. The development of many mushroom heads forms a cactus-like structure and very clumpy medium. ^{56}Ni is well mixed into the mushroom heads that extend to the outermost envelope. Technically, the mushroom structures depend strongly on the *mode* of the initial perturbation. The cactus-like structures are formed only when we introduce random perturbations. Such structures are the result of interactions between two or three mushrooms having a different direction of motion.

In Figure 4, the chemical compositions of He, C + O, and Si + Ni are plotted against M_r for run 4 with a sinusoidal perturbation (M20). This clearly shows the outward mixing of ^{56}Ni all the way to $M_r \sim 1.7\ M_\odot$, very close to the surface. At the same time, helium is mixed inward down to $M_r = 0.1\ M_\odot$.

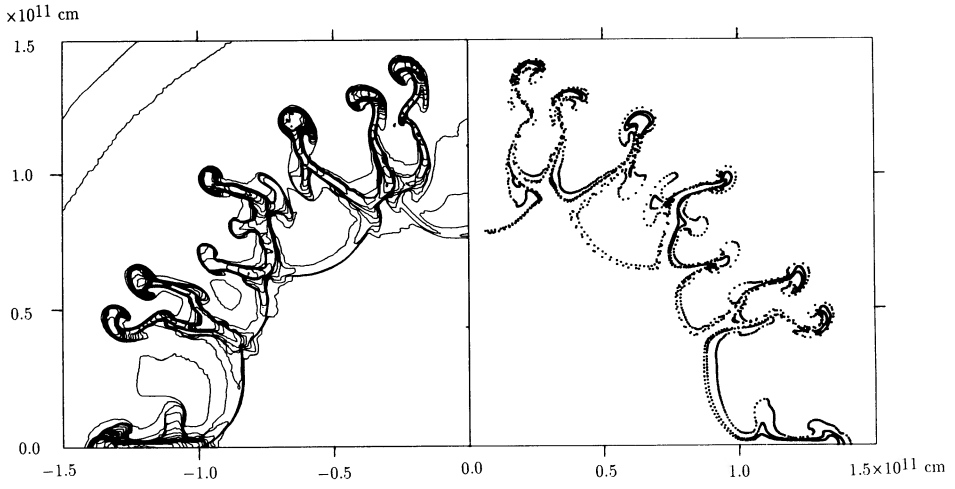

FIG. 3.—Same as Fig. 1 but for run 5 (2.1E1) at $t = 222$ s. The R-T instability develops most extensively among the calculated models. The plotted region is $1.5 \times 10^{11} \times 1.5 \times 10^{11}$ cm^2.

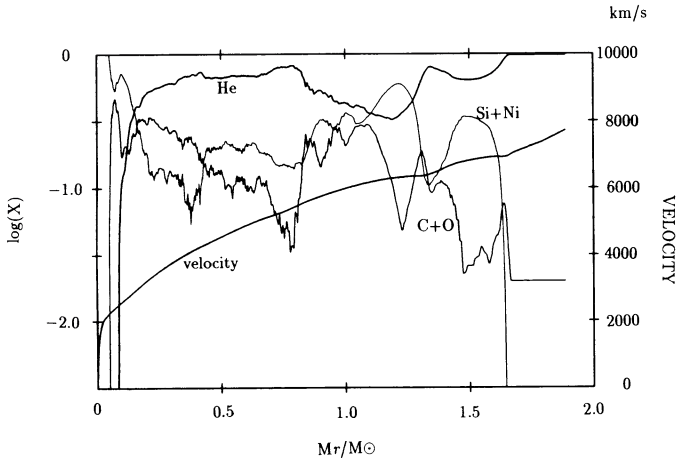

FIG. 4.—Chemical composition for run 4 (2.1E1) at $t = 180$ s is plotted against the radial mass coordinate, M_r. Mass fractions of He, C + O, and Si + Ni are shown by the thick, intermediate, and thin lines, respectively. The mean radial velocity is also shown (*thick solid line*). ^{56}Ni is mixed to the layer at $M_r = 1.7\ M_\odot$, i.e., $0.4\ M_\odot$ beneath the surface. A small part of the helium envelope ($\sim 0.2\ M_\odot$) has already moved out of the mesh.

4. CONCLUSIONS AND DISCUSSION

Our two-dimensional calculations clearly show that the R-T instabilities, being initiated at the He/C + O interface, induce more extensive mixing for smaller mass helium stars. For helium stars smaller than $\sim 5\ M_\odot$, mixing between the core and the envelope and the formation of clumps take place. On the contrary, almost no mixing or clump formation takes place for the $6\ M_\odot$ star (and for more massive stars). Such a mass dependence of the R-T instability is due to the difference in the stellar structure. For smaller mass stars, the mass ratio between the helium envelope and the heavy element mantle is larger (Table 1), which leads to larger deceleration of the core. Moreover, the density gradient at the He/C + O interface is steeper for smaller mass.

We should emphasize the importance of the density structure rather than the stellar mass itself. For example, a single Wolf-Rayet star which reduces its mass down to 4–5 $M_\odot$ by wind could be a SN Ib/Ic progenitor (Langer 1989). However, such a star would not undergo extensive mixing despite the small mass, because its helium envelope would be too small to largely decelerate the core material.

The extent of mixing found in the present calculations must be compared with that postulated in the light curve models for SN Ib/Ic (Shigeyama et al. 1990). In the two-dimensional simulation in 2.1E1 (2.7E1), ^{56}Ni is mixed to the layer at $0.4\ M_\odot$ ($1.6\ M_\odot$) beneath the surface. On the other hand, the calculated light curve of 2.1E1 (2.7E1) is in excellent agreement with SN 1987M (Type Ic) (SN 1983N [Type Ib]), if ^{56}Ni is mixed to the layer at $0.2\ M_\odot$ ($0.3\ M_\odot$) below the surface. Probably we need to include the effect of clumpiness in the next step of light curve modeling.

We conclude that the variation of mixing as a function of M_α found in the present study can naturally account for the variation of the SN Ib/Ic early light curves from the slow ones (SN Ib) to the fast ones (SN Ic) within the framework of helium star models. The spectral characteristics of SN Ic may be explained by the presence of hydrogen in SN Ic as recently identified in SN 1987M (Jeffery et al. 1990).

The computation was carried out on a Fujitsu VP-400E vector processor of the Data Processing Center of Kyoto University and on a VP-200 of the Institute of Space and Aeronautical Sciences (ISAS). This work has been supported in part by the Grant-in-Aid for Scientific Research (01540216, 01652506, 01790169, 02234206, 02302024, 02640204) of the Japanese Ministry of Education, Science, and Culture, the Space Data Analysis Center of ISAS, and the Japan-U.S. Cooperative Science Program (EPAR-071/88-15999) operated by the JSPS and the NSF.

REFERENCES

Arnett, W. D., Fryxell, B. A., & Müller, E. 1989, ApJ, 341, L63
Benz, W., & Thielemann, F.-K. 1990, ApJ, 348, L17
Den, M., Yoshida, T., & Yamada, Y. 1990, Progr. Theor. Phys., 83, 723
Ebisuzaki, T., Shigeyama, T., & Nomoto, K. 1989, ApJ, 344, L65
Ensman, L., & Woosley, S. E. 1988, ApJ, 333, 754
Filippenko, A. V., Porter, A. C., & Sargent, W. L. W. 1990, AJ, in press
Filippenko, A. V., & Sargent, W. L. W. 1989, ApJ, 345, L43
Fransson, C., & Chevalier, R. A. 1989, ApJ, 343, 323
Fryxell, B. A., Arnett, W. D., & Müller, E. 1991, ApJ, 367, 619
Goodman, J. 1990, ApJ, 358, 214
Hachisu, I., Matsuda, T., Nomoto, K., & Shigeyama, T. 1990, ApJ, 358, L57
Harkness, R. P., & Wheeler, J. C. 1990, in Supernovae, ed. A. Petschek (Berlin: Springer), p. 1
Hashimoto, M., Nomoto, K., & Shigeyama, T. 1989, A&A, 210, L5
Jeffery, D., Branch, D., Filippenko, A. V., & Nomoto, K. 1990, preprint
Kumagai, S., Shigeyama, T., Nomoto, K., Itoh, M., Nishimura, J., & Tsuruta, S. 1989, ApJ, 345, 412
Langer, N. 1989, A&A, 220, 135
Müller, E., Fryxell, B., & Arnett, W. D. 1990, in Chemical and Dynamical Evolution of Galaxies, ed. F. Ferrini, F. Matteucci, & J. Franco (Pisa: Casa Editrice Giardini), in press
Nomoto, K., Filippenko, A. V., & Shigeyama, T. 1990, A&A, in press
Nomoto, K., & Hashimoto, M. 1988, Phys. Rept., 163, 13
Nomoto, K., & Shigeyama, T. 1990, in Supernovae, ed. S. E. Woosley (Berlin: Springer), in press
Nomoto, K., Shigeyama, T., & Hashimoto, M. 1988, in IAU Colloquium 198, Atmospheric Diagnostics of Stellar Evolution, ed. K. Nomoto (Berlin: Springer), p. 319
Nomoto, K., Shigeyama, T., Kumagai, S., & Hashimoto, M. 1988, Proc. Astr. Soc. Australia, 7, 490
Panagia, N. 1987, in High Energy Phenomena around Collapsed Stars, ed. F. Pacini (Dordrecht: Reidel), p. 33
Schlegel, E. M., & Kirshner, R. P. 1989, AJ, 98, 577
Shigeyama, T., & Nomoto, K. 1990, ApJ, 360, 242
Shigeyama, T., Nomoto, K., & Hashimoto, M. 1988, A&A, 196, 141
Shigeyama, T., Nomoto, K., Tsujimoto, T., & Hashimoto, M. 1990, ApJ, 361, L23
Thielemann, F.-K., Hashimoto, M., & Nomoto, K. 1990, ApJ, 349, 222
Yamada, Y., Nakamura, T., & Oohara, K. 1990, Progr. Theor. Phys., in press